Impact of Soft Channel Construction on Iterative Channel Estimation and Data Decoding for Multicarrier Systems

Yao-Nan Lee[1], Alexei Ashikhmin*, Jiunn-Tsair Chen

Institute of Commun. Engr.
National Tsing Hua University
Hsinchu, Taiwan 30055, R.O.C.

*Math. of Communications Research Dep.
Bell Lab., Alcatel-Lucent Tech.
Murray Hill, NJ 07974, U.S.A.

July 26, 2007

Abstract

To apply the promising idea of iterative information processing to the problem of joint channel estimation and data decoding, one may utilize the soft information of the coded bits to help refine the channel estimate, e.g., with Wiener filtering. However, the performance of such an iterative approach depends on not only the construction of the iteratively refined soft channel, but also the structure of the adopted error-correction code. Through extrinsic information transfer chart analysis, we investigate the impact of different soft channel construction schemes on multicarrier systems possessing turbo coding/modulation structures: (1) one with bit-interleaved coded modulation signals, and (2) the other with low-density parity-check code encoded modulation signals. It is shown that the former benefits significantly from iterative information processing regardless of channel construction scheme and the performance of the systems with different schemes converges. On the contrary, the same observation cannot be applied to the latter, a capacity-approaching system.

Keywords: Iterative Process, Wiener Filter, Bit-Interleaved Coded Modulation, LDPC,

[1]Corresponding author, Email : ynlee@ieee.org, Return Address : Institute of Communications Engineering, National Tsing Hua University, Hsinchu, Taiwan 30055, R.O.C. TEL : +886 3 571-5131 ext 34145, FAX : +886 3 575-1787.

EXIT, Multicarrier.

1 Introduction

In most multicarrier wireless communication systems, estimating the channel response is a demanding task due to the limited number of pilot tones and high frequency selectivity of the wireless channels [1, 2]. Among the existing channel estimation techniques, those carried out in the frequency domain through interpolation with Wiener filtering [3], are believed to be simple and effective methods, which produce the optimum estimate of channel response in the sense of minimum mean-square error (MMSE). Moreover, soft information exchange between Wiener-filter-based channel estimator and error-correction decoder is generally expected to further purify the channel estimate. In this case, the channel estimator obtains help not only from the pilot symbols but also from the additional reliability information of the coded bits. However, we observe that iterative information processing between Wiener-filter-based channel estimator and error-correction decoder does not always improve the receiver performance, depending on 1) which family the adopted error-correction code is from, and 2) how we utilize the soft information of the coded bits at the Wiener-filter-based channel estimator.

The operation of the concerned multicarrier communication systems [4-8] can be summarized as follows: Making use of the initial channel estimation with the help of pilot symbols, the error-correction decoder decodes the receive signals and produces soft information of the coded bits. With these soft information, a temporary soft channel is constructed for a Wiener filter to refine the channel estimate followed by another round of error-correction decoding. Iterative information process between Wiener-filter-based channel estimator and error-correction decoder then proceeds.

In this paper, we investigate the impact of different soft channel construction schemes on receivers of two types of multicarrier communication systems with iterative channel estimation and data decoding: 1) one processing bit-interleaved coded modulation [9, 10] signals, 2) the other processing low-density parity-check code [11] encoded modulation signals. We name the receivers respectively as iterative CE-BICM receiver and iterative CE-LDPC re-

ceiver. Numerical experiments show that all soft channel construction schemes *significantly* benefit the performance of the iterative CE-BICM receivers and the bit error rate (BER) performance of the iterative CE-BICM receivers with different soft channel construction schemes converges when the signal-to-noise ratio is high. For the systems with the iterative CE-LDPC receivers, on the contrary, adopting different soft channel construction schemes may sometimes benefit *negligibly* or instead degrade the BER performance to a degree that is even worse than a non-iterative receiver. Furthermore, the BER performance of the iterative CE-LDPC receivers does not converge when the operating signal-to-noise ratio is high. Therefore, it should be careful when a capacity-approaching code is adopted in a communication system with iterative receivers. We shall explain all these phenomena through the extrinsic information transfer (EXIT) [12] chart later in this paper.

The rest of this paper is organized as follows. The system models are presented in Section 2. The impact of different soft channel construction schemes on Wiener-filter-based channel estimators is discussed in Section 3. The BER performance of the above-mentioned iterative receivers is analyzed in Section 4. Finally, a brief conclusion is drawn in Section 5.

2 System Model

In this section, we depict the model of the concerned multicarrier wireless communication systems with receivers handling iterative channel estimation and data decoding. First, Section 2.1 presents pilot symbol-assisted transmitters. Next, Section 2.2 describes an adopted wideband wireless channel model, and Section 2.3 explains the structure of the concerned iterative CE-BICM/CE-LDPC receivers.

2.1 Transmitters

For the transmitter corresponding to the iterative CE-BICM receiver, the bit sequence from a binary source is first encoded by a convolutional encoder. The encoded bit sequence is next *randomly* bitwise interleaved to increase the diversity order of the code [9, 10]. As for the transmitter corresponding to the iterative CE-LDPC receiver, the bit sequence from a binary

source is *directly* encoded by an LDPC encoder without an explicit bitwise interleaving, since the LDPC encoder has an embedded interleaver.

The interleaved coded bit sequence is grouped into a series of bit pairs $[c_{k,1}\, c_{k,2}]$, each of which is Gray-mapped onto the quadrature phase-shift-keying (QPSK) signals with alphabet $\{s_{00}, s_{01}, s_{10}, s_{11}\} = \{+1, +j, -1, -j\}$ to produce data symbols, where $c_{k,i}$ denotes the ith binary bit of the kth data symbol. After constellation mapping, pilot symbols are inserted every $L-1$ data symbols to form frequency-domain symbols $\{X_k\}$. These frequency-domain symbols are then modulated into K orthogonal subcarriers via an inverse fast Fourier transform and next padded with cyclic prefix to generate time-domain signals before going through a wireless channel.

Let us now define signal-to-noise ratio. Since the total energy of $(1 + C_{\mathrm{P}}) \cdot L \cdot E_{\mathrm{S}}$ carries only $2 \cdot (L-1) \cdot R_{\mathrm{C}}$ information bits, the average energy per information bit is given as

$$E_{\mathrm{b}} = \frac{(1 + C_{\mathrm{P}}) \cdot L \cdot E_{\mathrm{S}}}{2 \cdot (L-1) \cdot R_{\mathrm{C}}}, \tag{1}$$

where E_{S} is the average energy per data and pilot symbol, R_{C} is the code rate, and C_{P} is the ratio of cyclic prefix length to the total number of subcarriers K.

2.2 Wideband Wireless Channel Model

In this paper, we assume a wide-sense stationary uncorrelated scattering (WSSUS) channel model [13]. The time-varying frequency response of the wideband wireless channel can thus be expressed as

$$H(f,t) = \frac{1}{\sqrt{M}} \sum_{i=1}^{M} e^{j(\varphi_i + 2\pi f_{\mathrm{D},i} t - 2\pi f \tau_i)}, \tag{2}$$

where f and t are respectively continuous frequency and continuous time variables; φ_i, $f_{\mathrm{D},i}$, and τ_i are respectively the random phase, the Doppler spread, and the propagation delay of the ith path; and M denotes the total number of propagation paths. For simplicity, we assume that there is no Doppler spread.

As done in [13], the channel parameters φ_i and τ_i are independently generated according

to the following probability density functions:

$$p_{\varphi}(\varphi) = \begin{cases} \frac{1}{2\pi} & , 0 \leq \varphi \leq 2\pi \\ 0 & , \text{otherwise} \end{cases}, \tag{3}$$

and

$$p_{\tau}(\tau) = \begin{cases} \frac{e^{-\tau/\tau_{\text{rms}}}}{\tau_{\text{rms}}(1-e^{-\tau_{\max}/\tau_{\text{rms}}})} & , 0 \leq \tau \leq \tau_{\max} \\ 0 & , \text{otherwise} \end{cases}, \tag{4}$$

where $\tau_{\max}$ is the maximal channel delay spread and τ_{rms} is the root-mean-square delay spread chosen such that $p_{\tau}(\tau_{\max})/p_{\tau}(0) = 1/1000$. With the assumptions of these channel parameters, the complex autocorrelation function of the wideband channel response [6] in the frequency domain can be expressed as

$$R_k = \frac{1 - e^{-\tau_{\max}(\frac{1}{\tau_{\text{rms}}} + j2\pi \cdot k \cdot \triangle f)}}{(1 - e^{-\tau_{\max}/\tau_{\text{rms}}}) \cdot (1 + j2\pi \cdot k \cdot \triangle f \cdot \tau_{\text{rms}})}, \tag{5}$$

where $\triangle f$ is the sub-carrier spacing, and k is the discrete frequency index. The autocorrelation (5) will be used later in this paper to calculate the Wiener filter coefficients for MMSE channel estimation.

Assume that the length of the cyclic prefix is longer than the length of the maximal channel impulse response. After removing the cyclic prefix and performing multicarrier demodulation with fast Fourier transform, one can express the receive signal at the kth subcarrier as

$$Y_k = H_k \cdot X_k + Z_k, \tag{6}$$

where $H_k = H(k \cdot \triangle f, 0)$[1] is the discrete channel frequency response and Z_k is the additive noise assumed to be statistically independent and identically distributed complex Gaussian with mean being zero and variance being $\sigma^2 = \frac{N_0}{2}$ per dimension.

2.3 Iterative Receivers

Before describing the details of the iterative CE-BICM/CE-LDPC receivers, we first define an *observation window*. As shown in Fig. 1, when we intend to estimate the channel response at the hth subcarrier, the information that we are allowed to use is assumed within

[1]See (2). We assume that there is no Doppler spread throughput this paper.

a window defined as the observation window Ψ_h. Note that Ψ_h is also used to represent all the subcarrier indices within the observation window of the hth subcarrier. In the first-round pilot-aided channel estimation, all the information that helps estimate the channel response at a subcarrier is the available pilot symbols within the observation window of that subcarrier. On the other hand, in the subsequent iterative channel estimations, not only the available pilot symbols but also the soft information of the coded bits within the observation window help estimate the channel response. It seems intuitive that channel estimate *should* be greatly improved after iterative information processing begins, due to larger amount of available side information. Unfortunately, this intuition is not always true, as will be explained later.

2.3.1 Iterative CE-BICM Receivers

We now describe how to perform iterative channel estimation and data decoding with the iterative CE-BICM receiver shown in Fig. 2. In the first-round pilot-aided channel estimation, the channel estimates at all the pilot subcarriers $\left\{\tilde{H}_k\right\}$ can be obtained by dividing the receive signal Y_k with the known pilot symbol X_k where $k \in \Psi' \triangleq \left\{0, L, 2L, ..., L \cdot \lfloor \frac{K-1}{L} \rfloor\right\}$, and Ψ' denotes the set of subcarrier indices of all the pilot symbols. Note that the channel estimates obtained at all the pilot subcarriers will not be re-estimated and will be kept unchanged as the iterative process proceeds. On the other hand, the channel estimates at the data subcarriers can be obtained through a Wiener filter which employs an one-dimensional interpolation on those available channel estimates $\left\{\tilde{H}_k | k \in \Psi'_h\right\}$; where Ψ'_h, a subset of Ψ', contains the subcarrier indices of the pilot symbols within the observation window of the subcarrier h. We name the above Wiener filter as *pilot Wiener filter*. The first-round pilot-aided channel estimates can then be expressed as follows:

$$\hat{H}_{\mathrm{P},h} = \begin{cases} \tilde{H}_h = Y_h / X_h & , \text{ if } h \in \Psi' \\ (\underline{w}_{\mathrm{P},h})^T \cdot \underline{\tilde{H}}_{\mathrm{P},h} = \sum_{k \in \Psi'_h} w_{\mathrm{P},h,k} \cdot \tilde{H}_k & , \text{ if } 0 \le h \le K-1 \text{ and } h \notin \Psi' \end{cases}, \quad (7)$$

where $\underline{w}_{\mathrm{P},h} = \left[\left\{w_{\mathrm{P},h,k} | k \in \Psi'_h\right\}\right]^T$ is the coefficient column vector of the pilot Wiener filter, and $\underline{\tilde{H}}_{\mathrm{P},h} = \left[\left\{\tilde{H}_k | k \in \Psi'_h\right\}\right]^T$. Note that $\underline{w}_{\mathrm{P},h}$, $\underline{\tilde{H}}_{\mathrm{P},h}$ and Ψ'_h depend on the distribution of

pilot subcarriers relative to subcarrier h as depicted in Fig. 1. The filter coefficients $\underline{w}_{\mathrm{P},h}$ of the pilot Wiener filter are obtained by solving the well-known Wiener-Hopf equation [6, 14], which can be expressed as

$$(\underline{w}_{\mathrm{P},h})^T = \underline{r}^T_{H\tilde{H},h} \cdot R^{-1}_{\tilde{H}\tilde{H},h} \tag{8}$$

with

$$\underline{r}^T_{H\tilde{H},h} = \left[\left\{R_{h-k} | k \in \Psi'_h\right\}\right]^T, \tag{9}$$

and

$$\begin{aligned} R_{\tilde{H}\tilde{H},h} &= \begin{bmatrix} R_{\Psi'_h(1)-\Psi'_h(1)} + N_0 & R_{\Psi'_h(1)-\Psi'_h(2)} & \cdots & R_{\Psi'_h(1)-\Psi'_h(n_h)} \\ R_{\Psi'_h(2)-\Psi'_h(1)} & R_{\Psi'_h(2)-\Psi'_h(2)} + N_0 & \cdots & R_{\Psi'_h(2)-\Psi'_h(n_h)} \\ \vdots & \vdots & \ddots & \vdots \\ R_{\Psi'_h(n_h)-\Psi'_h(1)} & R_{\Psi'_h(n_h)-\Psi'_h(2)} & \cdots & R_{\Psi'_h(n_h)-\Psi'_h(n_h)} + N_0 \end{bmatrix} \\ &= \begin{bmatrix} R_0 + N_0 & R^*_L & \cdots & R^*_{(n_h-1)L} \\ R_L & R_0 + N_0 & \cdots & R^*_{(n_h-2)L} \\ \vdots & \vdots & \ddots & \vdots \\ R_{(n_h-1)L} & R_{(n_h-2)L} & \cdots & R_0 + N_0 \end{bmatrix}, \end{aligned} \tag{10}$$

where $\{R_k\}$ are defined in (5), $\Psi'_h(i)$ denotes the ith element of the ascending-ordered set Ψ'_h and n_h is the number of pilot symbols within the observation window of subcarrier h.

With the first-round pilot-aided channel estimates, we can now calculate the *a posteriori* log-likelihood values (L-values) $A_{\mathrm{CE}}(c_{k,i}) + E_{\mathrm{CE}}(c_{k,i})$ of the ith binary bit $c_{k,i}$ for the coded data symbol $X_k\,(c_{k,1}, c_{k,2})$ with a soft bit demapper, where $A_{\mathrm{CE}}(c_{k,i})$ and $E_{\mathrm{CE}}(c_{k,i})$ are the corresponding intrinsic and extrinsic L-values respectively. After deinterleaving, error-correction decoding with the BCJR algorithm [15] and interleaving, the new intrinsic L-values A_{CE} are then applied to the input of a channel re-constructor and a Wiener filter different from the previously-defined pilot Wiener filter so as to trigger subsequent channel estimation. We name the channel re-constructor and this Wiener filter respectively as *soft channel mapper* and *symbol Wiener filter*.

In addition to the information of the pilot symbols, we now have soft information of the coded bits A_{CE} from the error-correction decoder. Hence, we can further purify the channel

estimates. The soft channel mapper first constructs temporary soft channel estimates for all the subcarriers as follows:

$$\tilde{\mathrm{G}}_k = \begin{cases} \tilde{H}_k = Y_k / X_k & , \text{ if } k \in \Psi^{'} \\ f(Y_k, A_{\mathrm{CE}}(c_{k,1}, c_{k,2})) & , \text{ if } 0 \leq k \leq K-1 \text{ and } k \notin \Psi^{'} \end{cases} , \tag{11}$$

where the channel mapping function $f(Y_k, A_{\mathrm{CE}}(c_{k,1}, c_{k,2}))$ is a function of both the receive signal Y_k and the intrinsic L-values $A_{\mathrm{CE}}(c_{k,1}, c_{k,2})$ of the coded bits. The mapping function can be defined in different ways to construct the temporary soft channel for the symbol Wiener filter to refine the channel estimates. The impact of different channel mapping functions on the behavior of the Wiener-filter-based channel estimator will be discussed in Section 3. Now, the estimate of channel response at the hth subcarrier can be further purified with the symbol Wiener filter as follows:

$$\hat{H}_{\mathrm{S},h} = \begin{cases} \tilde{H}_h = Y_h / X_h & , \text{ if } h \in \Psi^{'} \\ (\underline{w}_{\mathrm{S},h})^T \cdot \underline{\tilde{H}}_{\mathrm{S},h} = \sum_{k \in \Psi_h \setminus \{h\}} w_{\mathrm{S},h,k} \cdot \tilde{\mathrm{G}}_k & , \text{ if } 0 \leq h \leq K-1 \text{ and } h \notin \Psi^{'} \end{cases} , \tag{12}$$

where $\underline{w}_{\mathrm{S},h} = [\{w_{\mathrm{S},h,k} | k \in \Psi_h \setminus \{h\}\}]^{\mathrm{T}}$ is the coefficient column vector of the symbol Wiener filter and $\underline{\tilde{H}}_{\mathrm{S},h} = \left[\left\{\tilde{\mathrm{G}}_k | k \in \Psi_h \setminus \{h\}\right\}\right]^T = \left[\tilde{\mathrm{G}}_{h-q}, \cdots, \tilde{\mathrm{G}}_{h-1}, \tilde{\mathrm{G}}_{h+1}, \cdots, \tilde{\mathrm{G}}_{h+q}\right]^{\mathrm{T}}$ with $2q$ being the tap length of the symbol Wiener filter, one tap less than the observation window length. Note that the symbol Wiener filter is also derived from the Wiener-Hopf equation making use of the temporary soft channel estimates of the subcarriers within the corresponding observation window. Detailed mathematical expressions of the symbol Wiener filter are similar to (8), (9) and (10), and are omitted here.

After purifying the channel estimates for all the subcarriers with symbol Wiener filter, we can again calculate the extrinsic L-values E_{CE} of the coded bits with the soft bit demapper and perform another round of error-correction decoding. Iterative channel estimation and data decoding thus proceeds.

2.3.2 Iterative CE-LDPC Receivers

Different from the iterative CE-BICM receiver, there are several different approaches to exchange soft information within an iterative receiver including an LDPC decoder as one

of its sub-blocks, since an LDPC decoder inherently has an internal turbo decoding cycle, in addition to the larger external CE/LDPC circle. Therefore, we analyze the performance of the iterative CE-LDPC receivers with two types of soft information exchange, as shown in Fig. 3: 1) the variable node decoder (VND) is firstly combined with the Wiener-filter-based channel estimator to form a super-VND as done in [16], and the soft information is exchanged between super-VND and CND, and 2) the soft information is exchanged along a larger external circle between Wiener-filter-based channel estimator and LDPC decoder, where the LDPC decoder can itself exchange soft information between VND and CND many times along a smaller internal circle between any two consecutive large-circle soft information exchange. We name the former as the first type CE-LDPC receiver, and the latter as the second type CE-LDPC receiver. Note that, in order to make the EXIT chart analysis feasible in the second type CE-LDPC receiver, $I_{\mathrm{E,LDPC}}$ should depend *only* on $I_{\mathrm{A,LDPC}}$, i.e. $I_{\mathrm{E,CE}}$. Therefore, we should *reset* $I_{\mathrm{A,VND}}$ when the channel estimator passes newly updated soft information to the LDPC decoder, as done in [17].

3 Behavior of the Channel Estimator with Different Mapping Functions

In this section, we describe three different ways to define the channel mapping function $f(Y_k, A_{\mathrm{CE}}(c_{k,1}, c_{k,2}))$, each of which can be used to construct a temporary soft channel for the symbol Wiener filter to refine the channel estimate. We then discuss their respective impact on the Wiener-filter-based channel estimator.

- Scheme-1: The temporary soft channel is constructed by dividing the receive signal Y_k with the soft symbol [5, 7], the mean value of the data symbol at the kth subcarrier, i.e.,

$$f(Y_k, A_{\mathrm{CE}}(c_{k,1}, c_{k,2})) = \frac{Y_k}{\sum_{i,j=\{0,1\}} p(s_{ij}) \cdot s_{ij}}, \tag{13}$$

where $p(s_{ij}) = p(c_{k,1} = i) \cdot p(c_{k,2} = j)$ with $p(c_{k,1} = i)$ and $p(c_{k,2} = j)$ as

$$\begin{cases} p(c_{k,1}=0) = \frac{1+\tanh(\frac{A_{\mathrm{CE}}(c_{k,1})}{2})}{2},\ p(c_{k,1}=1) = \frac{1-\tanh(\frac{A_{\mathrm{CE}}(c_{k,1})}{2})}{2} \\ p(c_{k,2}=0) = \frac{1+\tanh(\frac{A_{\mathrm{CE}}(c_{k,2})}{2})}{2},\ p(c_{k,2}=1) = \frac{1-\tanh(\frac{A_{\mathrm{CE}}(c_{k,2})}{2})}{2} \end{cases} . \tag{14}$$

- Scheme-2: The temporary soft channel can also be derived as the mean value of the channel response [6], i.e.,

$$f(Y_k, A_{\mathrm{CE}}(c_{k,1}, c_{k,2})) = \sum_{i,j=\{0,1\}} p(s_{ij}) \cdot \frac{Y_k}{s_{ij}}. \tag{15}$$

- Scheme-3: This approach gradually increases the influence of the soft information from the error-correction decoder and decreases the influence of the first-round pilot-aided channel estimate as the soft information iteratively purifies, i.e.,

$$f(Y_k, A_{\mathrm{CE}}(c_{k,1}, c_{k,2})) = \max_{p(s_{ij})} \left[p(s_{ij}) \cdot \frac{Y_k}{s_{ij}} \right] + [1 - p(s_{ij})] \cdot \hat{H}_{\mathrm{P},k}, \tag{16}$$

where $\hat{H}_{\mathrm{P},k}$ is the channel estimate obtained in the first-round channel estimation (7). A very similar approach like this one can be found in [8].

We next employ the extrinsic information transfer (EXIT) chart [12] to analyze the impact of these channel mapping functions on the Wiener-filter-based channel estimator. A well-designed signal-processing block is expected to have a monotonically increasing EXIT curve $I_{\mathrm{E}}(I_{\mathrm{A}})$. That is, the signal-processing block should produce higher output mutual information I_{E} if it is provided with a higher input mutual information I_{A}. Surprisingly, as shown in Figs. 5, 6, 11, and 12, we do not always obtain monotonically increasing EXIT curves for channel estimators with some channel mapping functions regardless of the operating signal-to-noise ratio. In other words, the soft information of the coded bits provided by the error-correction decoder do not always help improve the performance of the Wiener-filter-based channel estimator. Note that the "cross" in these figures marks the amount of extrinsic mutual information $I_{\mathrm{E,CE}}$ obtained in the *first round channel estimation* when $I_{\mathrm{A,CE}} = 0$, which is the same for the channel estimator with any of the three mapping functions, since the mapping function in the channel estimator has not come into play at this moment.

For the channel estimator with Scheme-1 mapping function, when $I_{\mathrm{A,CE}}$ is low, say $I_{\mathrm{A,CE}} \gtrsim 0$, the obtained soft symbol approaches zero since $p(s_{ij}) \approx 0.25$ for all i, j, which would then make the temporary soft channel $\{\tilde{\mathrm{G}}_k\}$ extremely large. This is why the mutual information at the output of channel estimator with Scheme-1 mapping function decreases to almost zero when $I_{\mathrm{A,CE}} \gtrsim 0$. The channel estimator with Scheme-2 mapping function can obtain higher output mutual information than that with Scheme-1 mapping function, since the temporary soft channel $\{\tilde{\mathrm{G}}_k\}$ constructed by Scheme-2 mapping function is zero when $I_{\mathrm{A,CE}} \gtrsim 0$, which incurs less deviation compared to that with Scheme-1 mapping function. Contrary to the channel estimator with Scheme-1 or Scheme-2 mapping function, the channel estimator with Scheme-3 mapping function well utilizes the first-round channel estimates and gradually increases the influence of the soft information of the coded bits from error-correction decoder. As observed in Figs. 5, 6, 11, and 12, this approach obtains a monotonically increasing EXIT curve even when $I_{\mathrm{A,CE}} \gtrsim 0$. In addition, one can easily find that the mathematical forms of the three different mapping functions in fact degenerate to the same function when $I_{\mathrm{A,CE}} = 1$, which makes the three corresponding EXIT curves coincide when $I_{\mathrm{A,CE}} = 1$. Based on the behavior of the EXIT curves above, we will analyze the BER performance for the iterative CE-BICM/CE-LDPC receivers in Section 4.

4 BER Analysis for Iterative Receivers

Some numerical BER performance results are obtained with the following system parameters: the number of total subcarriers $K = 1024$, the pilot symbol spacing $L = 12$, the code rate of both the convolutional code and the LDPC code $R_{\mathrm{C}} = \frac{1}{2}$, the number of coded bits in a codeword $n = 98580$ consisting of 53 OFDM symbols, the ratio of cyclic prefix $C_{\mathrm{P}} = \frac{1}{8}$, the number of propagation paths $M = 500$, the maximal delay spread $\tau_{\max} = 20\mu$sec, the observation window length $2q+1 = 41$, and the total number of codewords is 100, or roughly about 10^7 coded bits, for the simulation of each signal-to-noise ratio.

As for the operations in the receivers, we conduct 50 iterations between the channel estimator and the APP decoder in the iterative CE-BICM receiver; and the same number

of iterations between the super-VND and the CND in the first type CE-LDPC receiver. In addition, we set the number of iterations between VND and CND at 25 and set that between CE and LDPC decoder at 5 in the second type CE-LDPC receiver. More internal LDPC or more external CE/LDPC iterations hardly improve the BER performance in the second type CE-LDPC receiver. Note that the complexity of the second type CE-LDPC receiver is much higher than that of the first type CE-LDPC receiver when the number of the CE/LDPC iterations exceeds 2.

4.1 BER analysis of CE-BICM receiver

The convolutional code we use for the systems with CE-BICM receivers is the 16-state maximum-free-distance code adopted in the GSM standard [18]. In addition to the BER performance of the iterative CE-BICM receivers with different mapping functions, for comparison, we also evaluate the BER performance of a non-iterative CE-BICM receiver. The non-iterative CE-BICM receiver estimates the channel response only in the first round and then passes the L-values of the coded bits to the APP decoder for error correction without further iterative soft information exchange between channel estimator and APP decoder.

As shown in Fig. 4, the temporary soft channels constructed by all three mapping functions do improve the BER performance of the iterative CE-BICM receiver in median to high SNR regime. With any mapping function, the gain is about 2 dB for the iterative CE-BICM receiver as compared to the non-iterative CE-BICM receiver at BER $= 10^{-3}$, which confirms the contribution of all three mapping functions [5, 6, 7, 8]. When E_b/N_0 is above 6 dB, the BER performance of the iterative CE-BICM receivers with different mapping functions converges. However, the BER performance of the iterative CE-BICM receiver with Scheme-1 or Scheme-2 mapping function turns worse in low SNR regime as compared to the non-iterative CE-BICM receiver. These phenomena can be explained through the EXIT curves in Figs. 5 and 6.

After first-round channel estimation and error-correction decoding, the soft information from the APP decoder is unreliable if the operating signal-to-noise ratio is low. This unre-

liable soft information makes the EXIT curves of the Wiener-filter-based channel estimator with either Scheme-1 or Scheme-2 mapping function fall below the EXIT curve of the APP decoder, as shown in Fig. 5, which then degrades the BER performance of the iterative CE-BICM receiver.

On the other hand, the soft information from the APP decoder is more reliable after the first-round channel estimation and error-correction decoding if the operating signal-to-noise ratio is high enough, due to the chair-shaped EXIT curve of the APP decoder for the adopted convolutional code. This more reliable soft information makes the EXIT curves of the Wiener-filter-based channel estimator with any mapping function overcome the risk of early intersection with the EXIT curve of the APP decoder, as shown in Fig. 6. Since the tunnel between the EXIT curve of the APP decoder and that of the Wiener-filter-based channel estimator opens up, the iterative soft information exchange between channel estimator and APP decoder helps improve the BER performance of the iterative CE-BICM receiver. Note that the EXIT curves of the Wiener-filter-based channel estimators with all three mapping functions coincide when $I_{\mathrm{A,CE}}$ is close to one. This explains the BER performance of the iterative CE-BICM receivers with three mapping functions converge when they operate in median to high SNR regime.

4.2 BER analysis of the first type CE-LDPC receiver

The LDPC code we use for the system with CE-LDPC receivers is the check-regular LDPC code with VND polynomial $b_v(x) = 0.51162x^2 + 0.24962x^3 + 0.23876x^{13}$ and CND polynomial $b_c(x) = x^7$. Again, in addition to the BER performance of the first type CE-LDPC receivers with different mapping functions, we evaluate the BER performance of a non-iterative CE-LDPC receiver for comparison. The non-iterative CE-LDPC receiver estimates the channel response only in the first round and then passes the L-values of the coded bits to the LDPC decoder for error correction. Different from the APP decoder for convolutional codes, the LDPC decoder of the non-iterative CE-LDPC receiver performs iterative soft information exchange between VND and CND to further correct data errors. We set the number of

iterations within the LDPC decoder to 50 in the non-iterative CE-LDPC receiver.

The BER performance of the first type CE-LDPC receivers with different mapping functions and that of the non-iterative CE-LDPC receiver are shown in Fig. 7. Contrast to the CE-BICM receivers, only the first type CE-LDPC receiver with Scheme-3 mapping function can outperform the non-iterative CE-LDPC receiver, where the difference is about 1.8 dB at BER = 10^{-4}. The first type CE-LDPC receiver with Scheme-1 or Scheme-2 mapping function does not benefit from the iterative soft information exchange between super-VND and CND. Soft information exchange degrades the performance of the first type CE-LDPC receivers with Scheme-1 and Scheme-2 mapping functions by about 2.9 dB and 0.9 dB, respectively. Also contrast to the iterative CE-BICM receivers, the BER performance of the first type CE-LDPC receivers with different mapping functions does not converge even when the signal-to-noise ratio is high.

Next, we use the EXIT chart to explain the above observed phenomena in the first type CE-LDPC receivers. Since the EXIT curve of the Wiener-filter-based channel estimator with Scheme-1 or Scheme-2 mapping function does not monotonically increase, the EXIT curve of the corresponding super-VND does not monotonically increase, either. This makes the EXIT curve of the super-VND fall below the EXIT curve of the CND, as shown in Fig. 8-(a) and Fig. 8-(b), which degrades the BER performance of the first type CE-LDPC receivers. On the other hand, as shown in Fig. 8-(c), due to the monotonically increasing EXIT curve of the Wiener-filter-based channel estimator with Scheme-3 mapping function, the EXIT curve of the corresponding super-VND and the EXIT curve of the CND do not intersect, which makes such a receiver gradually achieve error-free performance as iterative information process proceeds. To avoid early intersection between the EXIT curves of the super-VND and the EXIT curve of the CND, as shown in Fig. 9, the first type CE-LDPC receivers with Scheme-1 and Scheme-2 mapping functions must operate at a much higher signal-to-noise ratio.

4.3 BER analysis of the second type CE-LDPC receiver

Similar to the performance comparison made in the first type CE-LDPC receivers, in addition to the BER performance of the second type CE-LDPC receivers with different mapping functions, we again evaluate the BER performance of a non-iterative CE-LDPC receiver for comparison. However, the number of iterations between VND and CND is set at 25 in this non-iterative CE-LDPC receiver to remain consistent with that in the second type CE-LDPC receivers. Fig. 10 shows the BER performance of the second type CE-LDPC receivers with different mapping functions, and that of the non-iterative CE-LDPC receiver. The properties we observe in Fig. 10 are summarized as follows:

- 1) Similar to the first type CE-LDPC receivers, the BER performance of the second type CE-LDPC receivers with different mapping functions does not converge at higher signal-to-noise ratio regime.

- 2) Contrast to the first type CE-LDPC receiver, all the variants of the second type CE-LDPC receiver can more or less benefit from iterative soft information exchange. However, despite much higher complexity on soft information exchange between channel estimator and LDPC decoder, the performance improvement of the second type CE-LDPC receiver with Scheme-1 or Scheme-2 mapping function to a non-iterative receiver is *not so significant* as that observed in the iterative CE-BICM receiver. The gain is only 0.2 dB, which is almost *negligible*.

- 3) The BER performance of the second type CE-LDPC receiver with Scheme-3 mapping function is 0.3 dB worse than that of the first type CE-LDPC receiver also with Scheme-3 mapping function, even though the complexity of the former is much higher.

The above phenomena will be explained next with EXIT curves in Figs. 11 and 12:

- 1) As in the case of the iterative CE-BICM receiver, after first-round channel estimation and error-correction decoding, the soft information from the LDPC decoder is unreliable if the operating signal-to-noise ratio is not high enough. This unreliable soft

information makes the EXIT curves of the Wiener-filter-based channel estimator with either Scheme-1 or Scheme-2 mapping function fall below or intersect with the EXIT curve of the LDPC decoder, as shown in Fig. 11, which makes the BER performance of second type CE-LDPC receiver with Scheme-1 or Scheme-2 mapping function much worse than that of second type CE-LDPC receiver with Scheme-3 mapping function.

- 2) On the other hand, with the EXIT curve of the capacity-approaching LDPC decoder being *nearly vertically straight* when $I_{\mathrm{A,LDPC}}$ is above some threshold, the extrinsic soft information of the LDPC decoder $I_{\mathrm{E,LDPC}}$ can be made *close to one*, if the extrinsic soft information from the *first-round channel estimation* $I_{\mathrm{E,CE}}$ is generated at a higher signal-to-noise ratio, as shown in Fig. 12. Therefore, the performance gain due to external soft information iteration is very limited as compared to that of the non-iterative CE-LDPC receiver, and the gain is only 0.2 dB, which is almost *negligible*. From the explanations above and by observing the EXIT curves shown in Fig. 12, it is very clear why the BER performance of the second type CE-LDPC receivers with Scheme-1 and Scheme-2 mapping functions converges to the same level at higher signal-to-noise ratio regime.

- 3) The reason making the BER performance of the second type CE-LDPC receiver worse than that of the first type CE-LDPC receiver, both with Scheme-3 mapping function, is because of our resetting the soft information $I_{\mathrm{A,VND}}$ to make the EXIT chart analysis feasible when the channel estimator passes newly updated soft information to the LDPC decoder in the second type CE-LDPC receiver. Obviously, the first type CE-LDPC receiver obtains richer soft information than that of the second type CE-LDPC receiver when their $I_{\mathrm{E,CE}}$ values are the same. However, to further investigate the influence of not resetting $I_{\mathrm{A,VND}}$ in the second type CE-LDPC receiver complicates the EXIT chart analysis, and is beyond the scope of this work.

5 Conclusions

In this paper, we investigate the effects of different channel mapping functions [5-8] on the Wiener-filter-based channel estimator through EXIT analysis. Not all the channel mapping functions are helpful for the symbol Wiener filter to refine the channel estimates. Performance improvement [5, 6] provided by iterative information process in the iterative CE-BICM receivers with Scheme-1 and Scheme-2 mapping functions is due to the chair-shaped EXIT curves of the APP decoder for the adopted convolutional code, which helps all the sub-blocks in a complementary way to improve the mutual information. On the other hand, the performance of an iterative receiver including a capacity-approaching LDPC code as one of its sub-blocks varies diversely, it depends on not only the behavior of all the sub-blocks but also the formation of the soft-information-exchanging cycles.

References

[1] J. K. Cavers, "An analysis of pilot symbol assisted modulation for Rayleigh fading channels," in *IEEE Trans. Veh Technol.*, vol. 40, pp. 686-693, Nov. 1991.

[2] S. Coleri, M. Ergen, A. Puri, and A. Bahai "Channel estimation techniques based on pilot arrangement in OFDM systems," *IEEE Trans. Broadcasting*, vol. 48, no. 3, pp. 223-229, Sep. 2002.

[3] P. Hoeher, S. Kaiser, and P. Robertson, "Two-dimensional pilot-symbol-aided channel estimation by Wiener filtering," in *IEEE Proc. ICASSP*, Munich, Germany, Apr. 1997, pp. 1845-1848

[4] H.-J. Su and E. Geraniotis, "Improved performance of a PSAM system with iterative filtering and decoding," in *Proc. 36th Annu. Allerton Conf. Commun., Control, and Computing*, Sep. 1998, pp. 156-166.

[5] M. C. Valenti and B. D. Woerner "Iterative channel estimation and decoding of pilot symbol assisted Turbo codes over flat-fading channels," *IEEE J. Sel. Areas Commun.*, vol. 19, no. 9, pp. 1697-1705, Sep. 2001.

[6] F. Sanzi, S. Jelting, and J. Speidel, "A comparative study of iterative channel estimators for mobile OFDM systems," *IEEE Trans. Wireless Commun.*, vol. 2, no. 5, pp. 849-859, Sep. 2003.

[7] H. Niu and J. A. Ritcey, "Iterative channel estimation and decoding of pilot symbol assisted LDPC coded QAM over flat fading channels," in *Proc. 36th Asilomar Conf. Signals, Syst. Comput.*, Pacific Frove, CA, Nov. 2003, vol. 2, pp. 2265-2269.

[8] Y. Huang and J. A. Ritcey, "Joint iterative channel estimation and decoding for bit-interleaved coded modulation over correlated fading channel," *IEEE Trans. Wireless Commun.*, vol. 4, no. 5, pp. 2549-2558, Sep. 2005.

[9] G. Caire, G. Taricco, and E. Biglieri, "Bit-interleaved coded modulation," *IEEE Trans. Inf. Theory*, vol. 44, no. 3, pp. 927-945, May 1998.

[10] A. Chindapol and J. A. Ritcey, "Design, analysis and performance evaluation for BICM-ID with square QAM constellations in Rayleigh fading channels," *IEEE J. Sel. Areas Commun.*, vol. 19, no. 5, pp. 944-957, May 2001.

[11] T.J. Richardson, M.A. Shokrollahi, and R.L. Urbanke "Design of capacity-approaching irregular low-density parity-check codes," *IEEE Trans. Inf. Theory*, vol. 47, pp. 619-637, Feb. 2001.

[12] S. ten Brink, "Convergence behavior of iteratively decoded parallel concatenated codes," *IEEE Trans. Commun.*, vol. 49, pp. 1727-1737, Oct. 2001.

[13] P. Hoeher, "A statistical discrete-time model for the WSSUS multipath channel," *IEEE Trans. Veh. Technol.*, vol. 41, no. 4, pp. 461-468, Nov. 1992.

[14] H. H. Hayes, *Statistical Digital Signal Processing and Modeling*, New York: Wiley, 1996.

[15] S. Lin and D. J. Costello, Jr., *Error Control Coding*, 2nd ed. Upper Saddle River, NJ: Prentice Hall, 2004.

[16] S. ten Brink, G. Kramer, and A. Ashikhmin, "Design of low-density parity-check codes for modulation and detection," *IEEE Trans. Commun.*, vol. 52, no. 4, pp. 670-678, Apr. 2004.

[17] Jilei Hou, Paul H. Siegel, and Laurence B. Milstein, "Design of multi-input multi-output systems based on low-density parity-check codes," *IEEE Trans. Commun.,* vol. 53, pp. 601-611, Apr. 2005.

[18] Lecture note (Chanper 10) of EE 379B, *Digital Communication 2: Coding,* Stanford university, available online: http://www.stanford.edu/class/ee379b/

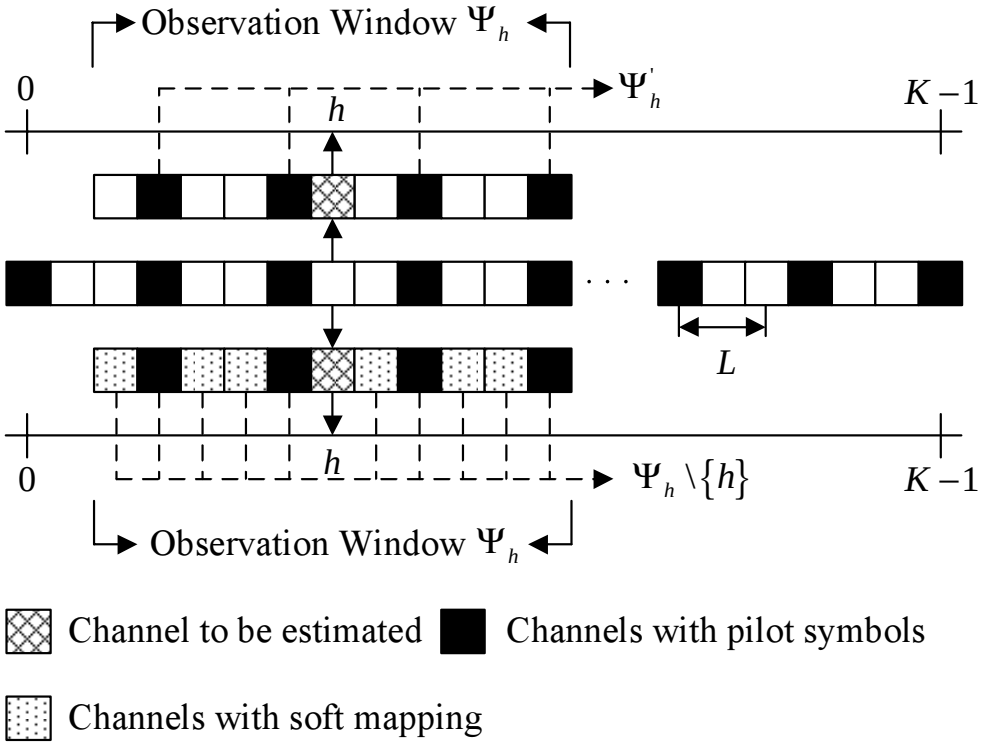


Figure 1: Relationship between observation window, inputs to the pilot Wiener filter Ψ'_h, and inputs to the symbol Wiener filter $\Psi_h \setminus \{h\}$.

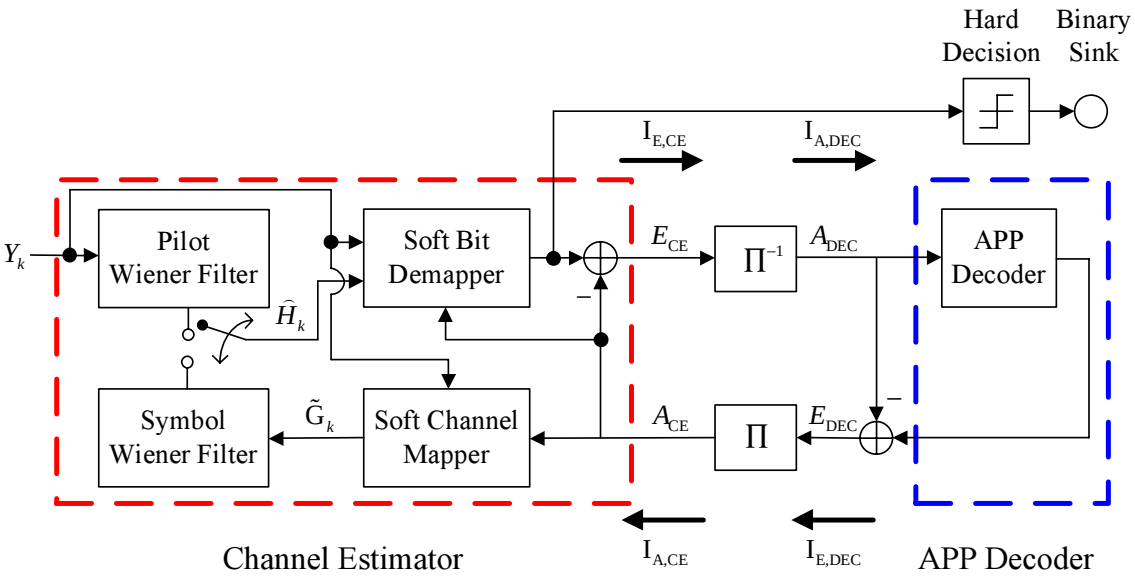


Figure 2: Block diagram of the receiver for iterative channel estimation and BICM decoding.

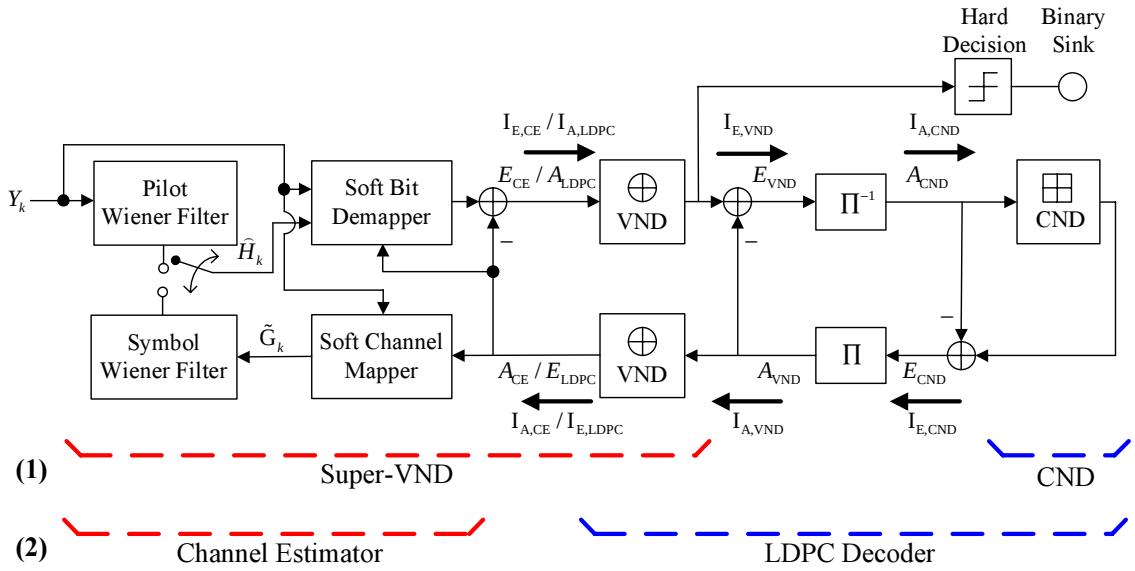


Figure 3: Block diagram of iterative CE-LDPC receiver with soft information exchange between 1) Super-VND and CND, or 2) Channel Estimator and LDPC Decoder.

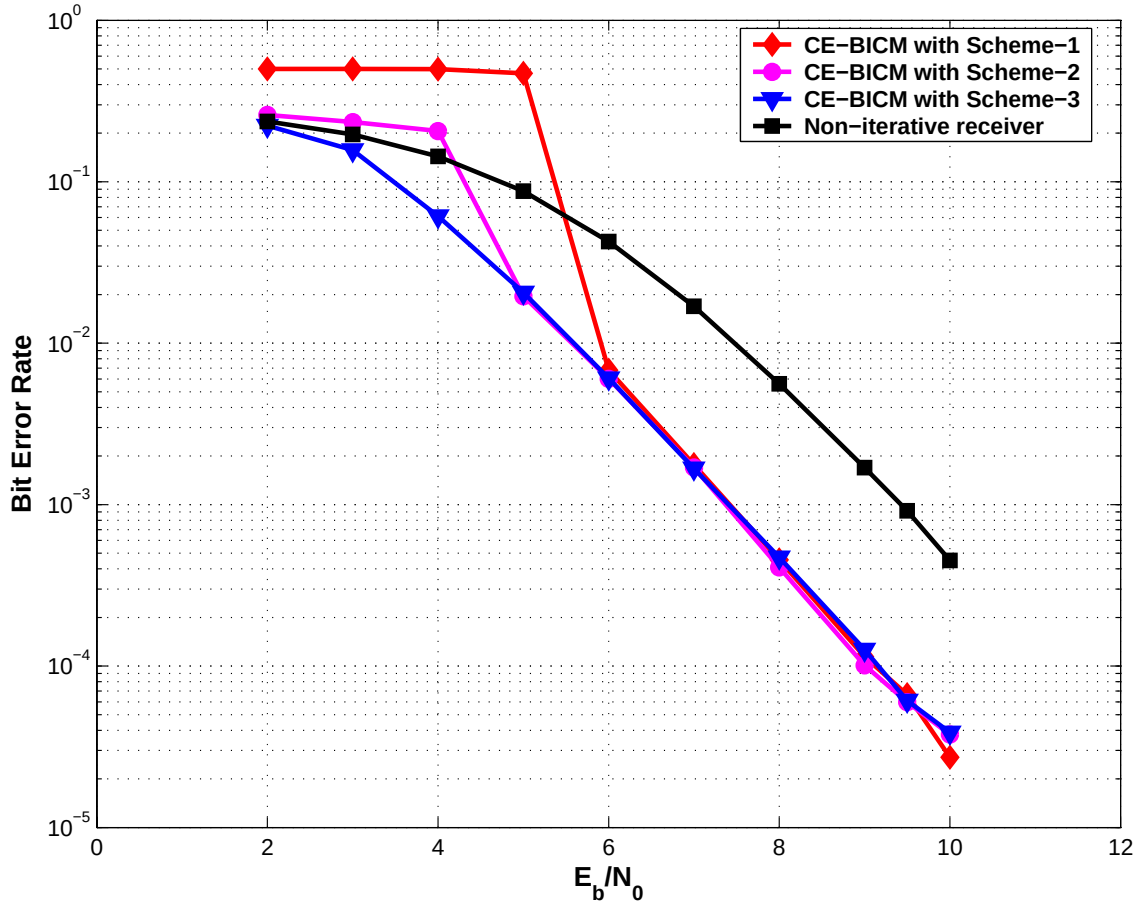


Figure 4: The BER performance of 1) the iterative CE-BICM receivers with different channel mapping functions and 2) the non-iterative CE-BICM receiver.

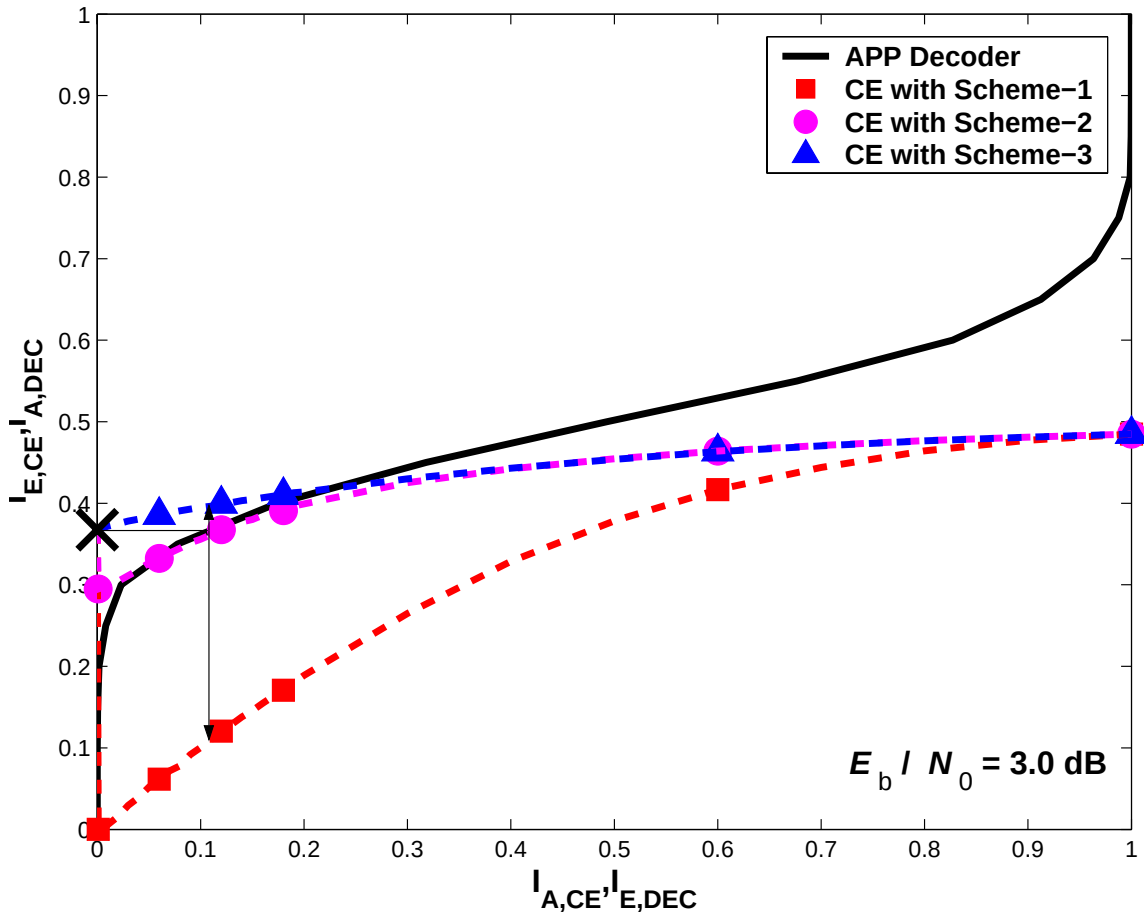


Figure 5: In the iterative CE-BICM receivers operating at a low signal-to-noise ratio, the EXIT curves of 1) the Wiener-filter-based channel estimators with different channel mapping functions and 2) the APP decoder.

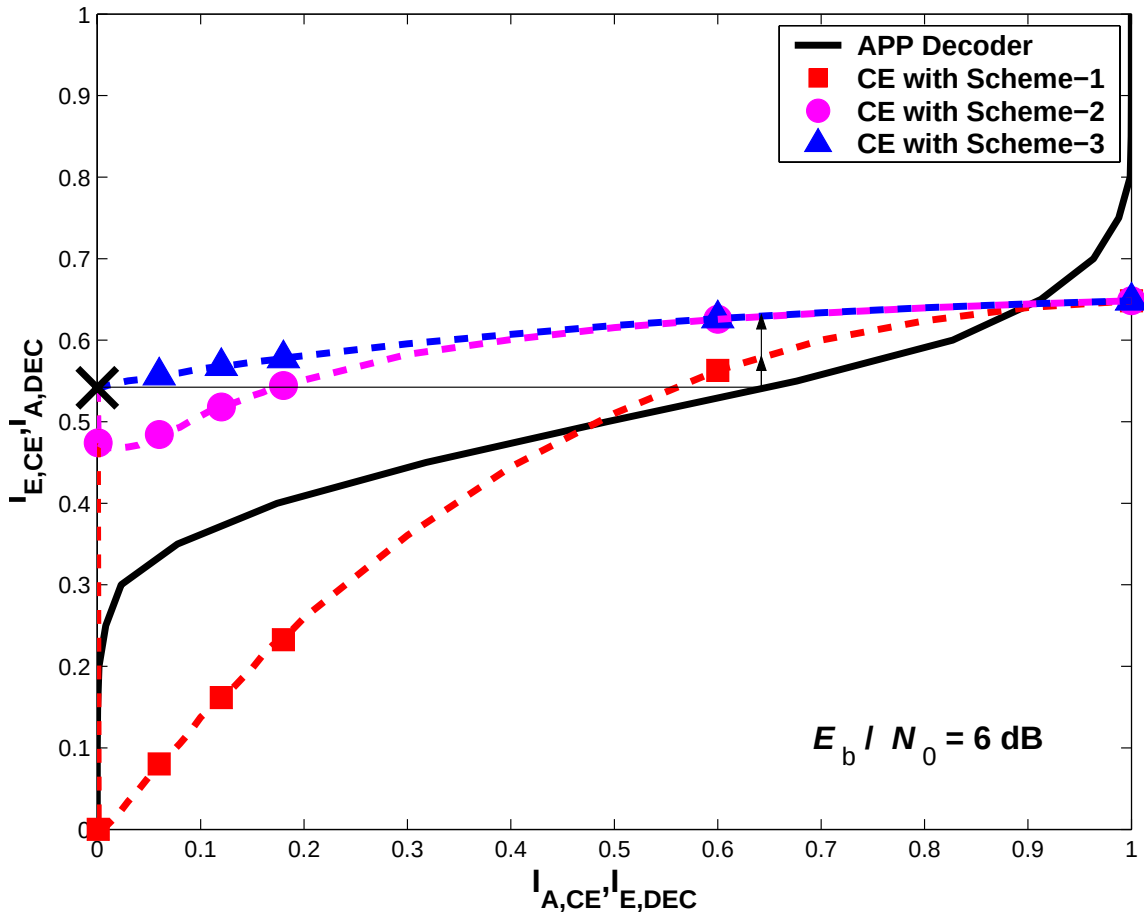


Figure 6: In the iterative CE-BICM receivers operating at a median signal-to-noise ratio, the EXIT curves of 1) the Wiener-filter-based channel estimators with different channel mapping functions and 2) the APP decoder.

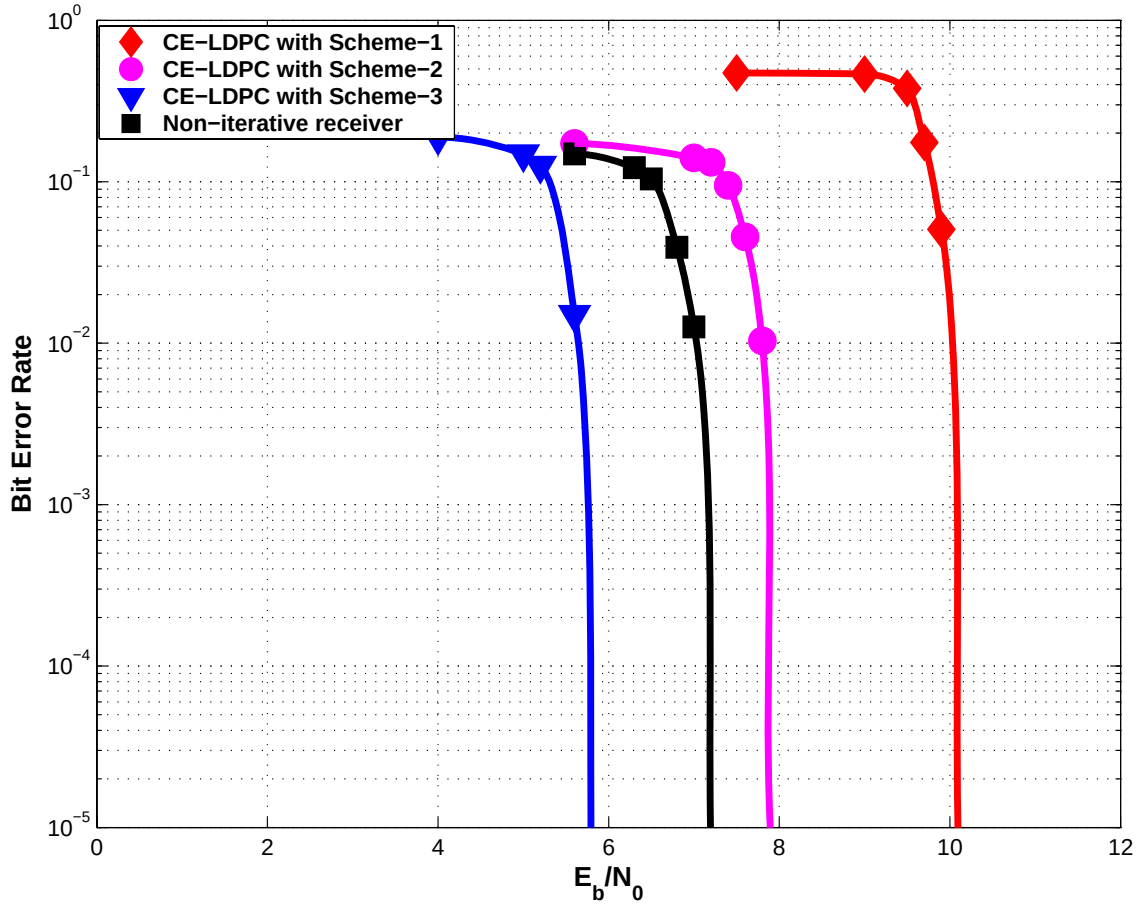


Figure 7: The BER performance of 1) the first type CE-LDPC receivers with different channel mapping functions and 2) the non-iterative CE-LDPC receiver.

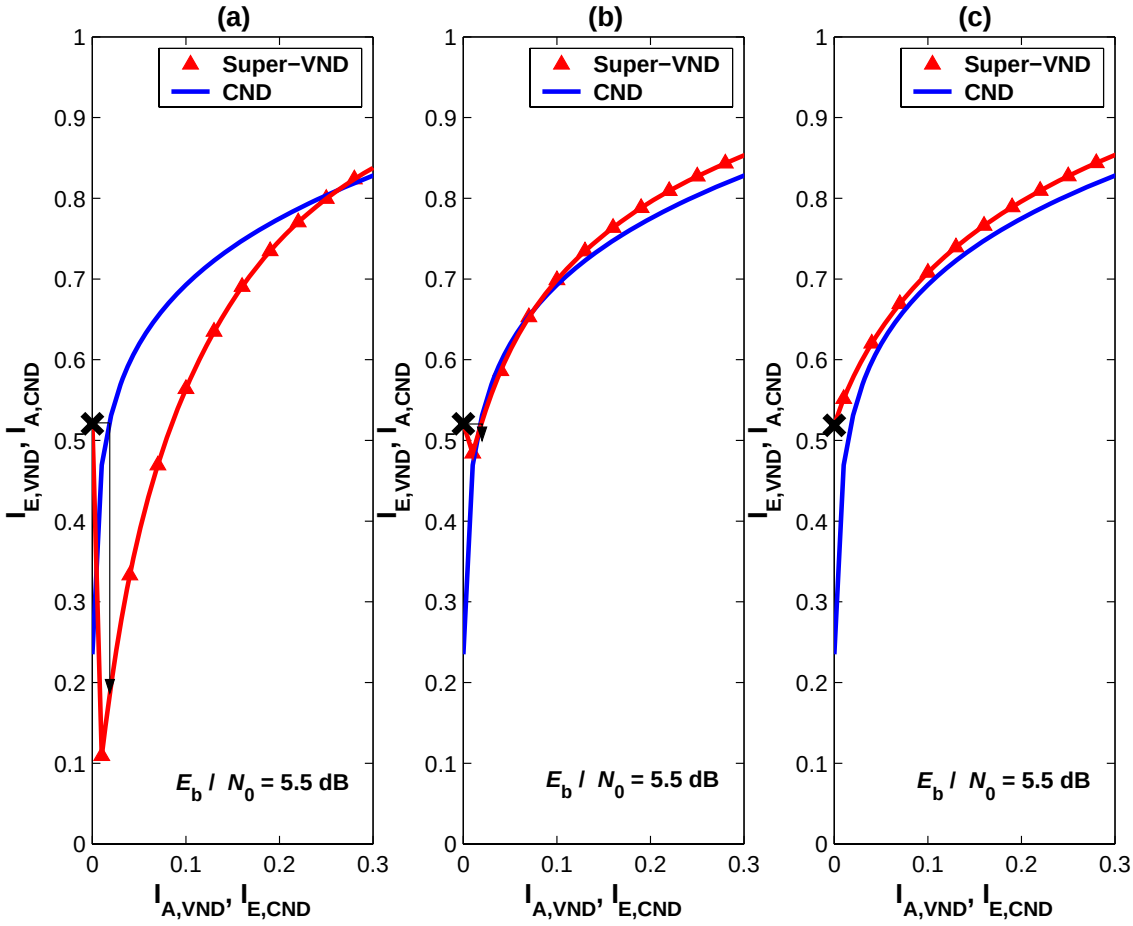


Figure 8: The EXIT charts of the first type CE-LDPC receivers with (a) Scheme-1, (b) Scheme-2, and (c) Scheme-3 channel mapping functions.

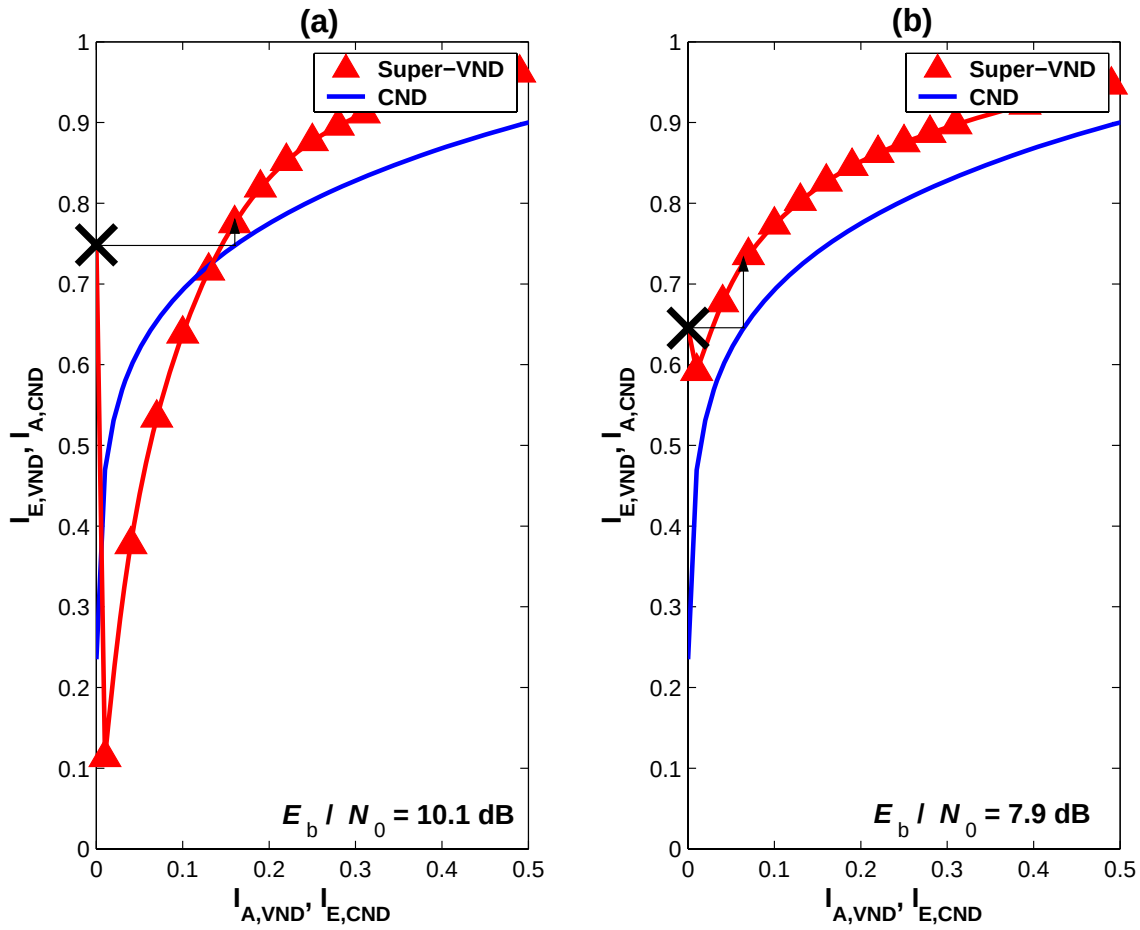


Figure 9: The EXIT charts of the first type CE-LDPC receivers with (a) Scheme-1 and (b) Scheme-2 channel mapping functions at a higher signal-to-noise ratio.

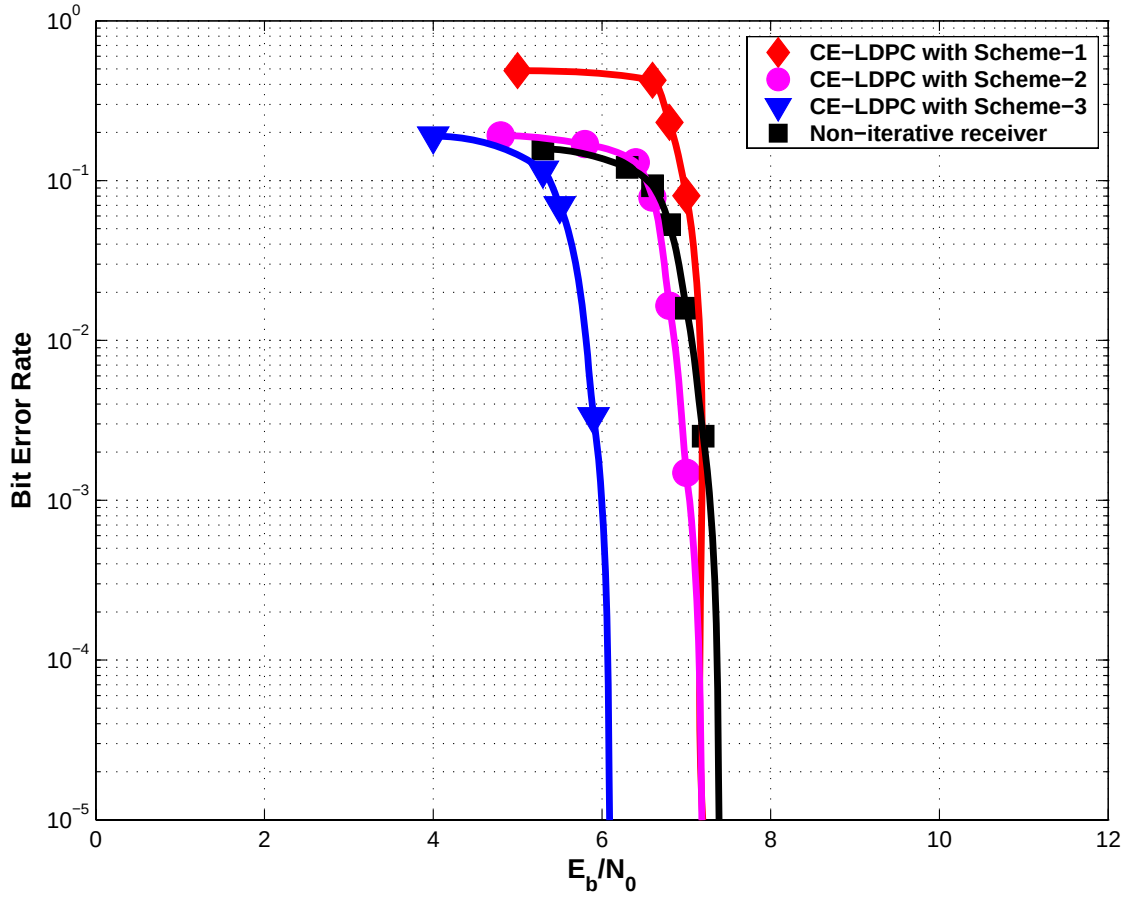


Figure 10: The BER performances of 1) the second type iterative CE-LDPC receivers with different mapping functions and 2) the non-iterative CE-LDPC receiver.

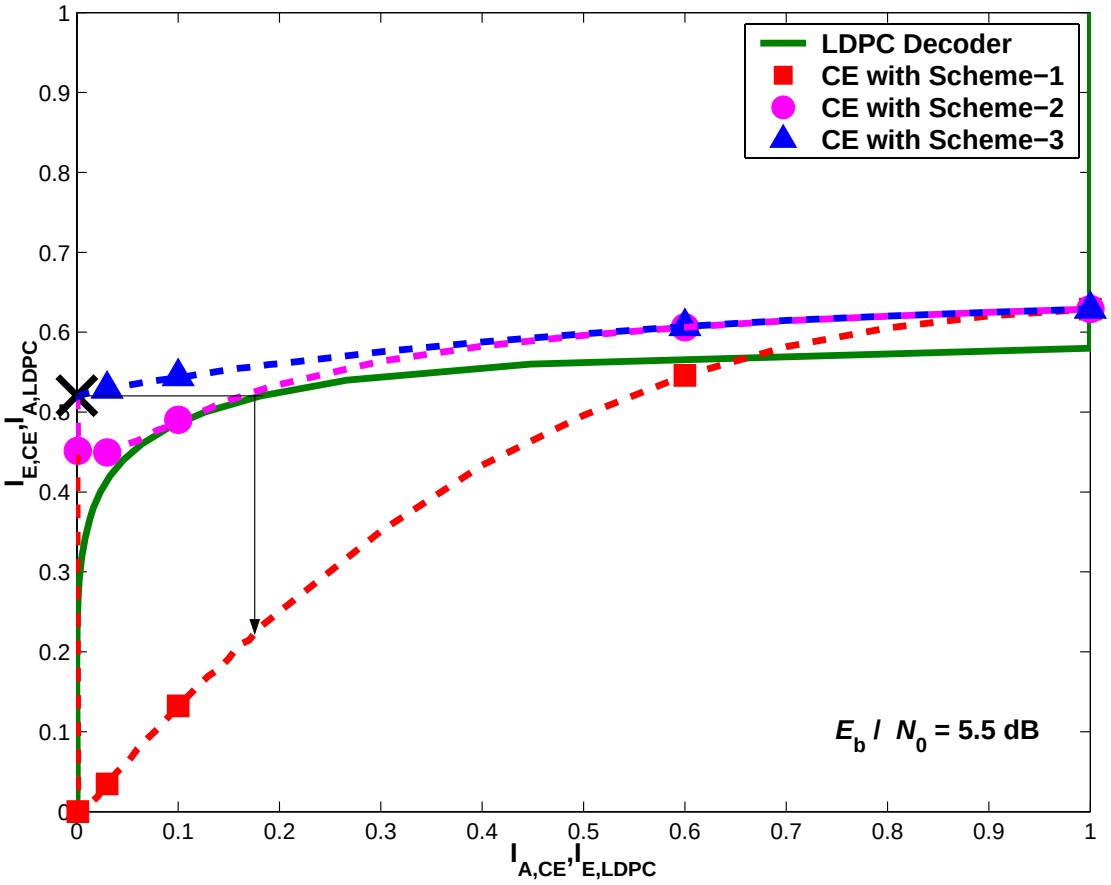


Figure 11: In the second type iterative CE-LDPC receivers operating at a median signal-to-noise ratio, the EXIT curves of 1) the Wiener-filter-based channel estimators with different mapping functions and 2) the LDPC decoder.

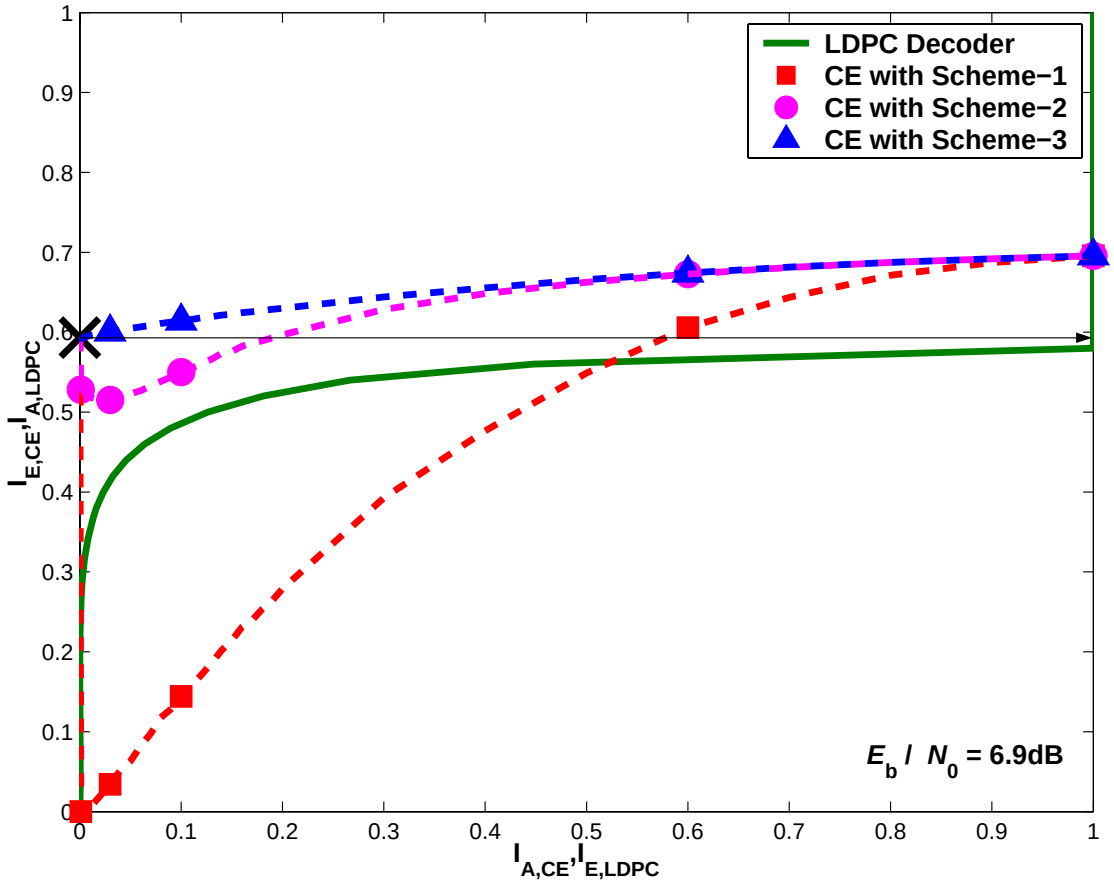


Figure 12: In the second type iterative CE-LDPC receivers operating at a higher signal-to-noise ratio, the EXIT curves of 1) the Wiener-filter-based channel estimators with different mapping functions and 2) the LDPC decoder.